World Academy of Science, Engineering and Technology
International Journal of Mechanical and Mechatronics Engineering
Vol:18, No:1, 2024

Optimal Sliding Mode Controller for Knee Flexion During Walking

Gabriel Sitler, Yousef Sardahi, Asad Salem

Abstract—This paper presents an optimal and robust sliding mode controller (SMC) to regulate the position of the knee joint angle for patients suffering from knee injuries. The controller imitates the role of active orthoses that produce the joint torques required to overcome gravity and loading forces and regain natural human movements. To this end, a mathematical model of the shank, the lower part of the leg, is derived first and then used for the control system design and computer simulations. The design of the controller is carried out in optimal and multi-objective settings. Four objectives are considered: minimization of the control effort and tracking error; and maximization of the control signal smoothness and closed-loop system's speed of response. Optimal solutions in terms of the Pareto set and its image, the Pareto front, are obtained. The results show that there are trade-offs among the design objectives and many optimal solutions from which the decision-maker can choose to implement. Also, computer simulations conducted at different points from the Pareto set and assuming knee squat movement demonstrate competing relationships among the design goals. In addition, the proposed control algorithm shows robustness in tracking a standard gait signal when accounting for uncertainty in the shank's parameters.

Keywords—Optimal control, multi-objective optimization, sliding mode control, wearable knee exoskeletons.

I. Introduction

THE motion of the shank relative to the upper leg, biomechanics behind the knee joint, and feasibility of wearable knee exoskeletons have been receiving much attention for two reasons: 1) knee injuries account for 41 % of all sports-related injuries [1], and 2) there is an increase in the number of elderlies who have difficulty standing and walking due to weak muscles and thus require assistance by supplying controlled torques via powered knee orthosis [2], [3].

Several control strategies for wearable knee exoskeletons during gait have been proposed. For instance, a nonlinear impedance reduction control (IRC) for minimizing human lower limb effort during gait was introduced in [4]. The control structure comprises three parts: a nonlinear joint torque observer, a nonlinear disturbance observer-based SMC, and desired admittance model. Theoretical analysis showed that the IRC performs quite well and it is robust against modeling uncertainties. Furthermore, experimental tests were conducted on four subjects and demonstrated that the IRC is quite effective through the acquisition of surface EMG signals. Another study presented an adaptive oscillator-based controller for a robotic lower-limb exoskeleton for patients who had difficulty walking or getting up without assistance due to weak muscles caused by aging [5]. Tests on two subjects demonstrated the feasibility of the proposed control strategy. Another study aimed at assisting elderly people during standing-up and walking by controlling the joint angle of wearable and actuated exoskeleton was proposed in [2]. PID and fuzzy controllers were used to control the exoskeleton actuators in this study. Computer simulations showed that the exoskeleton improves the motion and reduces the amount of torque required by the elderly. A tuned and a non-tuned PID algorithm for controlling the relative angular position of the shank with respect to the upper leg were introduced in [3]. Computer simulations of squat movement and normal gait revealed that the tuned PID provides smoother tracking.

In practice, the control design involves multiple requirements that are often conflicting. In the case of knee joint angle regulation, for example, the closed-loop system should be responsive and smooth, track the reference path fairly well, and use minimal control energy. Therefore, the control system design should be carried out in multi-objective settings to optimize the control performance and simultaneously address these design objectives. Both deterministic and stochastic multi-objective optimization methods have been proposed for this purpose. However, stochastic algorithms are more appealing due to their simplicity and the fact that they do not require smooth and convex cost functions, approximate global solutions well [6], and are noise resistant [7]. Dominant stochastic algorithms include the ACO (Ant Colony Optimization, [8]), MOGA (Multiple Objective Genetic Algorithm, [9]), PSO (Particle Swarm Optimization, [10]), NSGA-II, SPEA2 (Strength Pareto Evolutionary Algorithm, [11]), and NPGA-II (Niched Pareto Genetic Algorithm, [12]). The NSGA-II algorithm is the most widely used multi-objective optimization algorithm [13], [14]. According to [15], the algorithm outperforms the other methods in terms of Pareto front.

An extensive literature review proved that there is no literature on the design of a multi-objective and optimal control for knee joint angle during walking. As a result, the purpose of this paper is to introduce a multi-objective optimal SMC to control the position of the knee joint angle for people who have difficulty moving their legs due to injuries or aging. SMC is more effective than traditional PID controllers in controlling knee orthosis [16]. The NSGA-II tunes the SMC setup parameters to achieve minimum and smooth control effort, tracking error, and response time (1 % settling time).

The following is how this paper is structured. Section II introduces the shank's mathematical model. Section III details the design of the SMC. The multi-objective optimization problem is formulated in Section IV. Discussion of the optimization results is presented in Section V. Finally, Section

Gabriel Sitler is a graduate student, Dr.Sardahi is an Associate Professor and Dr.Salem is a Professor in the Mechanical Engineering program at Marshall University, USA (e-mail: sardahi@marshall.edu).

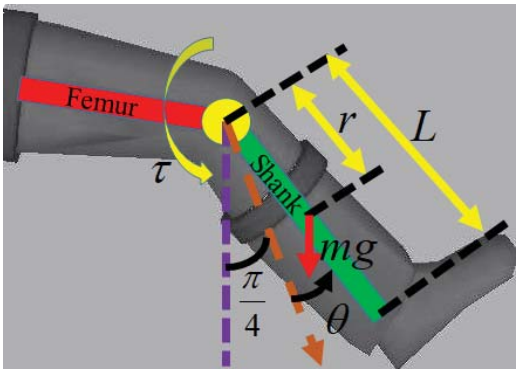

Fig. 1 Biomechanical model of the tibial movement [3]

VI contains our closing remarks.

II. Shank Mathematical Model

A pictorial representation of the shank biomechanical model when the patient is laying in a supine position is shown in Fig. 1. Following the work proposed in [3], we consider a 2D mathematical model of the shank movement, but only the movement in the sagittal plane, because the motions in the coronal plane are significantly smaller and can thus be ignored. The model features two segments: 1) the femur (the upper part of the leg) and 2) the shank (the lower part of the leg). The femur and shank are joined by a revolute joint that is powered by the torque τ, which mimics the torque applied to the knee joint by the orthoses. In this paper, τ denotes the control signal applied to the model. The angle θ represents the shank angular position relative to the middle range of motion ($\pi/4$), where the full range of motion is $\pi/2$. That is, $\theta = 0$ indicates that the shank is at the middle range of motion, while $\theta = \pi/4$ corresponds to the position when the shank is at its full extension. The model parameters and their values are listed in Table I, where m, L, r, and g are the shank mass, shank length, distance from the shank center of mass to the knee joint axis, and gravitational acceleration, respectively.

TABLE I
Model Parameters

Model Paramter	Value
m	3.72 kg
g	9.8 m/s^2
r	0.188 m
L	0.435 m
I	0.44 kgm^2
B	6.75 Nms/rad
K	44.22 Nm/rad

Applying Newton's second law for rotational mechanical systems, the dynamics of the shank model when the subject is laying in a supine position reads

$$I\ddot{\theta}(t) + B\dot{\theta}(t) + K\theta(t) + mgr\sin(\theta + \frac{\pi}{4}) = \tau(t) \quad (1)$$

Here, I, B, and K denote the shank inertia around the knee joint, the viscous damping coefficient of the knee joint, and the stiffness coefficient of the knee joint, respectively. Table I contains the values for these parameters.

III. SMC Design

The first step in designing of an SMC is to select the type and order of what is called the sliding mode surface (SMS) such that the system under control remains on it and slides to its stable equilibrium according to the dynamics specified by this surface. In the second step, a reaching law is chosen to ensure that the SMS is reached from a non-zero initial condition. For control system design purposes, (1) is re-written as

$$\ddot{\theta}(t) = f(\theta, \dot{\theta}) + Au(t), \quad (2)$$

where, $f(\theta, \dot{\theta})$ is given by

$$f(\theta, \dot{\theta}) = 1/I(-B\dot{\theta}(t) - K\theta(t) - mgr\sin(\theta + \frac{\pi}{4})). \quad (3)$$

The control signal $u(t) = \tau(t)$ and A is $1/I$. The control law $u(t)$ can be derived by first constructing the SMS, $s(t)$, which is given by:

$$s(t) = k_p e(t) + \dot{e}(t), \quad (4)$$

Here, we choose a proportional-derivative (PD) SMS. Although an SMS with an integral term may improve SMC robustness and tracking, it is not considered because the accumulation of tracking errors during rehabilitation training may eventually result in injuries to the subject wearing the orthosis [17]. In this equation, k_p is the SMS proportional gain that must satisfy the Hurwitz condition, $k_p > 0$. The tracking error $e(t)$ and its first-time derivative read

$$e(t) = \theta(t) - \theta_d(t) \quad (5)$$

$$\dot{e}(t) = \dot{\theta}(t) - \dot{\theta}_d(t), \quad (6)$$

where $\theta(t)$ is the actual angular position of the joint and $\theta_d(t)$ is the desired. To derive the control law $u(t)$, we first derive the expression $\dot{s}(t)$,

$$\begin{aligned} \dot{s}(t) &= k_p\dot{e}(t) + \ddot{e}(t) \\ &= k_p\dot{e}(t) + \ddot{\theta}(t) - \ddot{\theta}_d(t) \\ &= k_p\dot{e}(t) + f(\theta, \dot{\theta}) + Au(t) - \ddot{\theta}_d(t) \end{aligned} \quad (7)$$

Second, we choose a reaching law such that the time derivative of the Lyapunov function ($V = (1/2)s^2$) is negative and thus the closed loop system is stable. That is, the condition $s\dot{s} < 0$ is satisfied. To this end, the exponential reaching law, which is given by (8), is selected.

$$\dot{s} = -\mu sign(s) - k_e s, \quad \mu > 0, k_1 > 0, \quad (8)$$

where, μ and k_e are tunable parameters and must be non-negative to ensure closed-loop system stability. The exponential reaching law is chosen because it outperforms both constant and power rate reaching laws [18]. In practical applications, the $sign(s)$ function is usually replaced by the saturation function $sat(s)$ to alleviate chattering [19], [20], where $sat(s)$ is given by

$$sat(s) = \begin{cases} 1, & s > \Delta \\ ks, & |s| \leq \Delta \\ -1, & s < -\Delta \end{cases} \quad (9)$$

where $k = \frac{1}{\Delta}$, and the Δ is called the boundary layer. Replacing $sign(s)$ by $sat(s)$ and solving for $u(t)$, the control law reads

$$u(t) = \frac{1}{A}[-k_p\dot{e}(t) - f(\theta,\dot{\theta}) + \ddot{\theta}_d(t) \\ -\mu sat(s) - k_e s]. \tag{10}$$

It is obvious that k_p, μ, k_e, and Δ determine the required control effort and, as a result, affect the overall closed-loop system performance. Furthermore, these parameters should be optimally tuned to meet the requirements of the control system design.

IV. Multi-objective Optimization Problems

Because of their numerous practical applications, MOPs have received a lot of attention. A MOP is defined mathematically as

$$\min_{\mathbf{k}\in D}\{\mathbf{F}(\mathbf{k})\}, \tag{11}$$

where $\mathbf{F}$ is the map that consists of the objective functions $f_i : D \to \mathbb{R}^1$ under consideration.

$$\mathbf{F} : D \to \mathbb{R}^k,\ \mathbf{F}(\mathbf{k}) = [f_1(\mathbf{k}), \ldots, f_k(\mathbf{k})]. \tag{12}$$

$\mathbf{k} \in D$ is a d-dimensional vector of design parameters. The domain $D \subset \mathbb{R}^d$ can in general be expressed by inequality and equality constraints:

$$D \ = \{\mathbf{k} \in \mathbb{R}^d \mid g_i(\mathbf{k}) \le 0,\ i = 1, \ldots, l, \\ \text{and } h_j(\mathbf{k}) = 0,\ j = 1, \ldots, m\}. \tag{13}$$

In MOPs, the concept of *dominancy* [21] is usually used to define the optimal solutions. Such solutions dominate all the other solutions but do not dominate each other.

A. Multi-objective Optimal Design of SMC

Three pieces of information need to be defined for any MOP. They are the decision vector, objective space, and constraints. The decision vector is given by

$$\mathbf{k} = [k_e, \mu, k_p, \Delta]. \tag{14}$$

The constraints on the design gains are given by:

$$Q = \{\mathbf{k} \in \ [0.1, 10] \times [0.1, 10] \times \\ [0.1, 10] \times [0.0001, 0.1] \subset \mathbb{R}^4\}. \tag{15}$$

The lower limits of the parameters were set according to the constraints defined in (4) and (8) and the upper limits were arbitrary selected. The design objective space is stated as

$$\min_{\mathbf{k}\in Q}\{E_u, S_u, J_{IAE}, t_s\}, \tag{16}$$

where, E_u and S_u are the objectives that describe the control energy and its smoothness. They are provided by:

$$E_u = \int_0^t u^2(\tau)d\tau, \tag{17}$$

$$S_u = \frac{1}{n}\left\|u_{0:n-1} - u_{1:n}\right\|_1, \tag{18}$$

where $\|.\|$denotes the L_1 norm and n is the size of samples. The cost functions t_s and J_{IAE} are respectively the 1% settling time and the integral absolute error which is given by,

$$J_{IAE} = \int_0^t |\theta(\tau) - \theta_d(\tau)|d\tau, \tag{19}$$

To solve this multi-optimization problem, NSGA-II is used. More information about this algorithm can be found in [22]. There is no explicit instruction on how to configure the number of populations and generations for this algorithm. However, according to the MATLAB documentation, the population size can be configured in a variety of ways, with the default population size being 15 multiplied by the number of design variables $nvar$. Furthermore, the maximum number of generations should not exceed $200 \times nvar$. In this study, the population size and the number of generations are set to $200 \times nvar$. Following the work proposed in [3], we assume that the subject is performing a squat movement, which is defined as $\theta_d(t) = (\pi/4)sin(2\pi t)$. The amplitude is set to $\pi/4$ to cover θ range of motion, which is between 0 and $\pi/2$. Since the average time of a step in normal conditions is about 1 second [23], the period of θ_d is set to 1.

V. Results and Discussion

The output of NSGA-II in terms of the Pareto set and its image (Pareto front), the controlled system response to a squat movement and registered gait input, and the robustness of the Pareto front to parametric variations are discussed here.

The Pareto set and front are shown in Figs. 2 and 3, respectively. The color code in the figures represents the levels of S_u where the orange and dark blue colors represent respectively the highest and lowest levels. The color code provides better visualization for the Pareto set and shows the corresponding regions on the Pareto front. The Pareto set shows that smooth control signals are associated with small control gains as is evident by the color in the figure. In SMC, less chattering is achieved by increasing the boundary layer, Δ, of the $sat(s)$ function. However, Fig. 2 shows that even at $\Delta = 0.1$, the control signal can be non-smooth as long as μ, k_p, and k_e are big. This is also clear by the color code in Fig. 3 where large control values (E_u) are associated with large variations (S_u) in the control signal. The figure also demonstrates conflicting relationships between E_u and each of t_s and J_{IAE}. For example, when $E_u = 1550.67$, t_s and J_{IAE} read 1.18 and 0.202, respectively. On the other side, at the largest control effort, $E_u = 5161.85$, t_s and J_{IAE} are respectively 0.4 and 0.031. The Pareto front also record competing relationships among S_u, t_s, and J_{IAE}. For instance, when the switching in the control signal is the lowest, $S_u = 1.60$, t_s and J_{IAE} read 0.85 and 0.124, respectively. On the other side, when the switching in the control signal is the highest, $S_u = 2.71$, t_s and J_{IAE} are respectively 0.4 and 0.031.

A. Response to a Squat Movement

The conflict among the design objectives can be also demonstrated by the system response under the SMC at

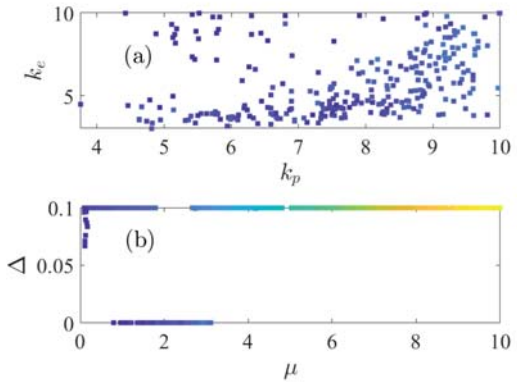

Fig. 2 2D visualization of the Pareto set; the color coding is mapped to the normalized value of S_u such that blue is the lowest and orange is the highest

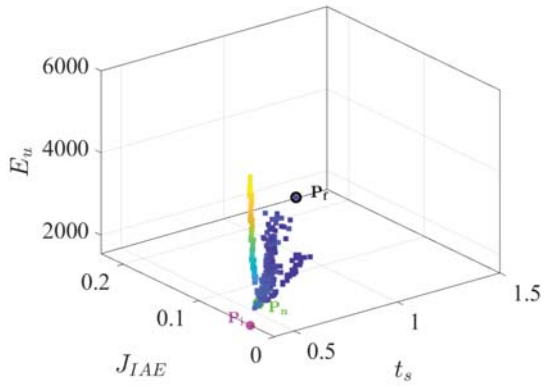

Fig. 3 3D visualization of the Pareto front; the color coding is mapped to the normalized value of S_u such that blue is the lowest and orange is the highest; $\mathbf{P_i}$, $\mathbf{P_n}$, and $\mathbf{P_f}$ are the ideal, knee, and far point, respectively.

different points. Here, we choose to show the response at $min(t_s)$ and $max(t_s)$ (see Fig. 4), $min(J_{IAE})$ and $max(J_{IAE})$ (see Fig. 5), $min(E_u)$ and $max(E_u)$, depicted in Fig. 6; and $min(S_u)$ and $max(S_u)$ (refer to Fig. 7) when the subject is doing a squat movement. The figures show that when the system speed of response is high and the trajectory tracking is the best (Figs. (4)-a, (5)-a, (6)-b, and (7)-b), E_u and S_u are at their highest values as demonstrated by the numerical values in the captions of these figures. On the other side, controlled system responses that are slow and have large tracking errors occur at small control effort and thus small variations in the control signal as shown in Figs. (4)-b, (5)-b, (6)-a, and (7)-a.

Three points are labeled on the Pareto front. The point $\mathbf{P}_i$ marks the location where all cost functions are the smallest and is thus an ideal solution not on the Pareto frontier while $\mathbf{P}_n$ is called the knee point and is the closest to $\mathbf{P}_i$ compared to the other point on the Pareto front. $\mathbf{P}_f$ is a point on the Pareto front and the furthest from $\mathbf{P}_i$. From an implementation perspective, $\mathbf{P}_n$ could be more attractive to the decision-maker

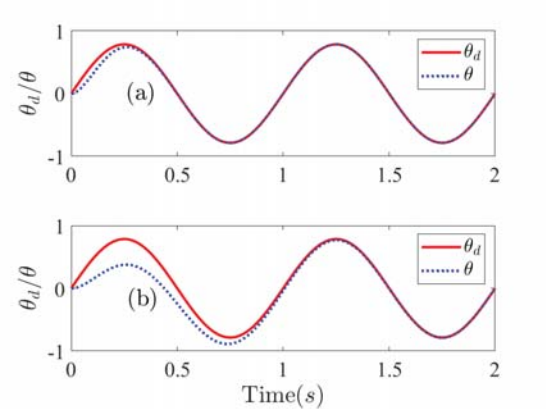

Fig. 4 Closed-loop response to a squat movement at (a) min (t_s) where $[k_e, \mu, k_p, \Delta] = [9.987211, 9.982392, 9.992594, 0.099795]$ and $[E_u, S_u, J_{IAE}, t_s] = [5158.772796, 2.712251, 0.031567, 0.400000]$, and (b) max (t_s) where $[k_e, \mu, k_p, \Delta] = [4.491859, 1.903205, 3.750269, 0.000106]$ and $[E_u, S_u, J_{IAE}, t_s] = [1572.877423, 1.623880, 0.229350, 1.350000]$

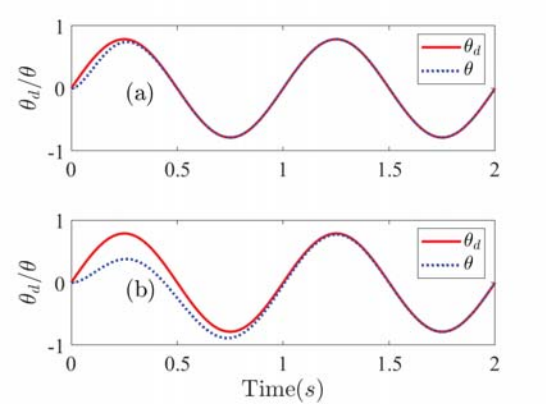

Fig. 5 Closed-loop response to a squat movement at (a) min (J_{IAE}) where $[k_e, \mu, k_p, \Delta] = [9.987289, 9.989739, 9.989376, 0.099794]$ and $[E_u, S_u, J_{IAE}, t_s] = [5161.856626, 2.713218, 0.031565, 0.400000]$, and (b) max (J_{IAE}) where $[k_e, \mu, k_p, \Delta] = [4.491859, 1.903205, 3.750269, 0.000106]$ and $[E_u, S_u, J_{IAE}, t_s] = [1572.877423, 1.623880, 0.229350, 1.350000]$

than $\mathbf{P}_f$ since it is the closest to the ideal solution. These two points explain the properties of the Pareto front. The response of the closed-loop system to a registered gait input at these points is discussed next.

B. Response to Gait Input

In addition to testing the controller response to squat movement, the second set of simulations was conducted to examine the response to a normal gait movement. The normal

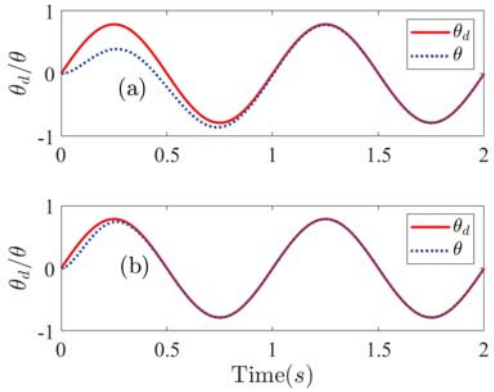

Fig. 6 Closed-loop response to a squat movement at (a) min (E_u) where $[k_e, \mu, k_p, \Delta] = [3.574013, 2.922288, 4.632296, 0.000106]$ and $[E_u, S_u, J_{IAE}, t_s] = [1550.679241, 1.722696, 0.202041, 1.180000]$, and (b) max (E_u) where $[k_e, \mu, k_p, \Delta] = [9.987289, 9.989739, 9.989376, 0.099794]$ and $[E_u, S_u, J_{IAE}, t_s] = [5161.856626, 2.713218, 0.031565, 0.400000]$

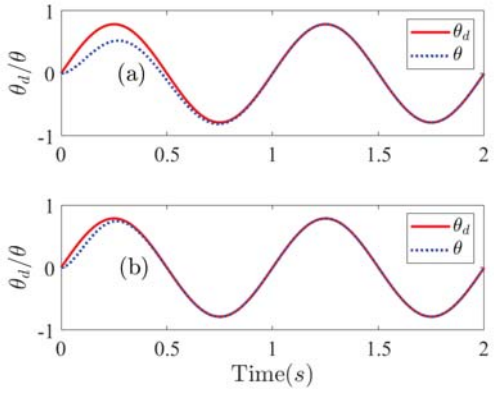

Fig. 7 Closed-loop response to a squat movement at (a) min (S_u) where $[k_e, \mu, k_p, \Delta] = 4.278734, 1.185731, 7.755477, 0.000105]$ and $[E_u, S_u, J_{IAE}, t_s] = [1613.472496, 1.602372, 0.124205, 0.850000]$, and (b) max (S_u) where $[k_e, \mu, k_p, \Delta] = [9.987289, 9.989739, 9.989376, 0.099794]$ and $[E_u, S_u, J_{IAE}, t_s] = [5161.856626, 2.713218, 0.031565, 0.400000]$

gait signal was created using a piecewise defined function that contained two sine functions that were set to interchange at 0.5 second intervals, in an attempt to mimic the reference gait signal in [3]. The response of the controller was observed at $\mathbf{P}_n$ and $\mathbf{P}_f$. From Fig. 8, it is clear that $\mathbf{P}_n$ has the better response, taking around 0.59 seconds to track the gait signal. On the other side, the controlled system response at $\mathbf{P}_f$ takes about 1.18 second to be within $\pm 1\%$ of the desired trajectory. To put it another way, the control algorithm successfully tracks the reference signal in both cases. However, the control effort at $\mathbf{P}_n$ is bigger than that at $\mathbf{P}_f$ as evident in Fig. 9 and by the objective values reported in the caption of Fig. 8.

C. Robustness to Parametric Variations

In realistic applications, the shank parameters will not be consistent in every person, so the controller needs to be capable of producing accurate responses for a variation of parameters. To account for uncertainty in shank parameters from one person to another, random values of each model parameter were generated using a normal Gaussian distribution for each of I, B, K, L, r, and m with the mean parameters set as the predefined shank parametric values, and a standard deviation of ±20% of each given mean parameter [24]. At each time point, 100 runs were performed, resulting in 100 uncertainty values of each parameter, at minimum energy cost $(min(E_u))$, where the robustness of the controlled system is the weakest. Then the controller response for the uncertainty values and mean values was compared to the normal gait signal as shown in Fig. 10. It can be noted that the control algorithm is robust against parametric variation, and the response matches the gait signal at just over 0.5 seconds and closely replicates the response speed we obtained for the predefined shank parameters.

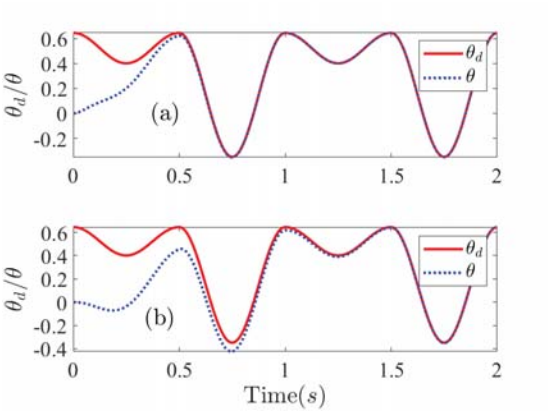

Fig. 8 Closed-loop response to normal gait at (a) $\mathbf{P_n}$ where $[k_e, \mu, k_p, \Delta] = 9.160440, 1.862266, 9.184981, 0.000105]$ and $[E_u, S_u, J_{IAE}, t_s] = [2068.580991, 2.619800, 0.134704, 0.590000]$, and (b) $\mathbf{P_f}$ where $[k_e, \mu, k_p, \Delta] = 4.491859, 1.903205, 3.750269, 0.000106]$ and $[E_u, S_u, J_{IAE}, t_s] = [1790.875131, 2.554519, 0.252310, 1.180000]$

VI. Concluding Remarks

In conclusion, the SMC designed in optimal and multi-objective settings performs well and produces a closed-loop response that tracks the knee joint angle effectively for both squat movement and normal gait. The optimization results display optimal and trade-off controllers from which the decision-maker can select. Furthermore, the proposed control method is robust against parametric

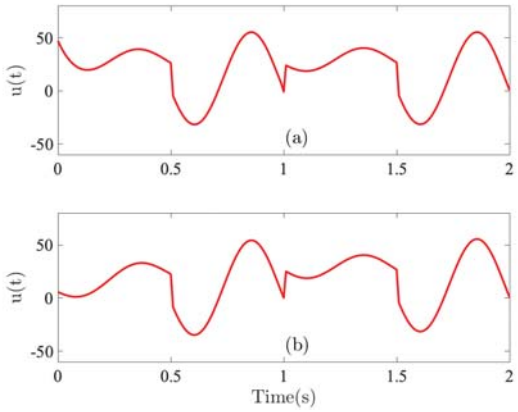

Fig. 9 Control signal with respect to time at (a) $\mathbf{P_n}$ and (b) $\mathbf{P_f}$

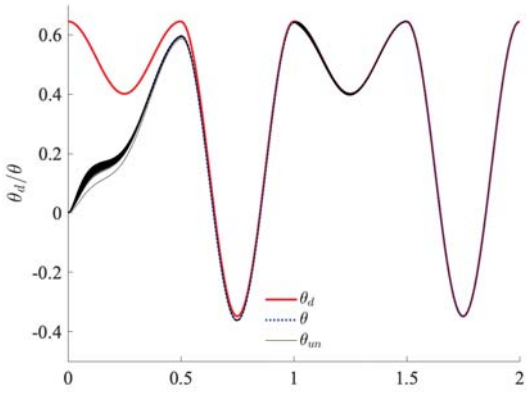

Fig. 10 Closed-loop response to normal gait at $min(E_u)$ with an uncertainty of shank parameters showing the 100 runs of θ_{un} in relation to θ_d and θ

uncertainty. However, some work still needs to be done to incorporate the dynamics of orthoses into control design and computer simulations.

REFERENCES

[1] P. K. Sancheti, M. Razi, E. B. Ramanathan, and P. S.-H. Yung, "Injuries around the knee – symposium," *British Journal of Sports Medicine*, vol. 44, pp. i1 – i1, 2010.

[2] D. Miranda-Linares, G. Alrezage, and M. Tokhi, "Control of lower limb exoskeleton for elderly assistance on basic mobility tasks," in *2015 19th International Conference on System Theory, Control and Computing (ICSTCC)*. IEEE, 2015, pp. 441–446.

[3] A. Chevalier, C. M. Ionescu, and R. De Keyser, "Model-based vs auto-tuning design of pid controller for knee flexion during gait," in *2014 IEEE International Conference on Systems, Man, and Cybernetics (SMC)*. IEEE, 2014, pp. 3878–3883.

[4] W. Huo, S. Mohammed, and Y. Amirat, "Impedance reduction control of a knee joint human-exoskeleton system," *IEEE Transactions on Control Systems Technology*, vol. 27, no. 6, pp. 2541–2556, 2018.

[5] K. Seo, K. Kim, Y. J. Park, J.-K. Cho, J. Lee, B. Choi, B. Lim, Y. Lee, and Y. Shim, "Adaptive oscillator-based control for active lower-limb exoskeleton and its metabolic impact," in *2018 IEEE International Conference on Robotics and Automation (ICRA)*. IEEE, 2018, pp. 6752–6758.

[6] T. Erfani and S. V. Utyuzhnikov, "Directed search domain: a method for even generation of the pareto frontier in multiobjective optimization," *Engineering Optimization*, vol. 43, no. 5, pp. 467–484, 2011.

[7] O. M. Shir, S. Chen, D. Amid, D. Boaz, A. Anaby-Tavor, and D. Moor, "Pareto optimization and tradeoff analysis applied to meta-learning of multiple simulation criteria," in *2013 Winter Simulations Conference (WSC)*. IEEE, 2013, pp. 89–100.

[8] G. Reinelt, *The traveling salesman: computational solutions for TSP applications*. Springer-Verlag, 1994.

[9] C. M. M. D. Fonseca, "Multiobjective genetic algorithms with application to control engineering problems." Ph.D. dissertation, University of Sheffield, 1995.

[10] J. Moore and R. Chapman, "Application of particle swarm to multiobjective optimization," *Department of Computer Science and Software Engineering, Auburn University*, vol. 32, 1999.

[11] E. Zitzler, M. Laumanns, and L. Thiele, "SPEA2: Improving the strength pareto evolutionary algorithm," *TIK-report*, vol. 103, 2001.

[12] M. Erickson, A. Mayer, and J. Horn, "The niched Pareto genetic algorithm 2 applied to the design of groundwater remediation systems," in *International Conference on Evolutionary Multi-Criterion Optimization*. Springer, 2001, pp. 681–695.

[13] Y. Sardahi and A. Boker, "Multi-objective optimal design of four-parameter PID controls," in *ASME 2018 Dynamic Systems and Control Conference*. American Society of Mechanical Engineers, 2018, pp. V001T01A001–V001T01A001.

[14] X. Xu, Y. Sardahi, and C. Zheng, "Multi-objective optimal design of passive suspension system with inerter damper," in *ASME 2018 Dynamic Systems and Control Conference*. American Society of Mechanical Engineers, 2018, pp. V003T40A006–V003T40A006.

[15] B. Gadhvi, V. Savsani, and V. Patel, "Multi-objective optimization of vehicle passive suspension system using NSGA-II, SPEA2 and PESA-II," *Procedia Technology*, vol. 23, pp. 361–368, 2016.

[16] M. Ashmi, M. Anila, and K. Sivanandan, "Comparison of SMC and PID controllers for pneumatically powered knee orthosis," *Journal of Control, Automation and Electrical Systems*, vol. 32, no. 5, pp. 1153–1163, 2021.

[17] J. Cao, S. Q. Xie, and R. Das, "Mimo sliding mode controller for gait exoskeleton driven by pneumatic muscles," *IEEE Transactions on Control Systems Technology*, vol. 26, no. 1, pp. 274–281, 2017.

[18] X. Xu, Y. Sardahi, and A. Boker, "Multi-objective optimal design of a PID sliding mode controller with three different reaching laws," in *Dynamic Systems and Control Conference*, vol. 59155. American Society of Mechanical Engineers, 2019, p. V002T25A002.

[19] B. Janardhanan and S. Spurgeon, "Advances in sliding mode control: Concept, theory and implementation," 2013.

[20] J. Liu and X. Wang, *Advanced sliding mode control for mechanical systems: design, analysis and MATLAB simulation*. Springer Science & Business Media, 2012.

[21] V. Pareto, *Manual of Political Economy*. London: The MacMillan Press, 1971 (original edition in French in 1927).

[22] K. Deb, *Multi-Objective Optimization Using Evolutionary Algorithms*. New York: Wiley, 2001.

[23] Y. Liu, K. Lu, S. Yan, M. Sun, D. K. Lester, and K. Zhang, "Gait phase varies over velocities," *Gait & posture*, vol. 39, no. 2, pp. 756–760, 2014.

[24] M. Al-Fandi, M. A. K. Jaradat, and Y. Sardahi, "Optimal PI-fuzzy logic controller of glucose concentration using genetic algorithm," *International Journal of Knowledge-based and Intelligent Engineering Systems*, vol. 15, no. 2, pp. 99–117, 2011.

Gabriel Sitler is a graduate student in the Department of Mechanical and Industrial Engineering at Marshall University. He plays as a Goalkeeper in the men's soccer team. His research interest includes the control system design of wearable knee exoskeletons.

Dr. Yousef Sardahi is an associate professor in the Department of Mechanical and Industrial Engineering at Marshall University. He earned a Ph.D. from the Department of Mechanical Engineering at the University of California, Merced, in 2016. His research interest includes Control System Design and Multi-Objective Optimization.

Dr. Asad Salem is the Director of Recruitment and Accreditation at the College of Engineering and Computer Science and Professor of Mechanical Engineering in the Department of Mechanical Engineering at Marshall University. His research interest includes: Thermal Science, Computational Fluid Dynamics (CFD), Finite Elements, Renewable and Sustainable Energy Sources such as Wind and Solar, Co-generation, Cryogenic Thermodynamics Cycles, LNG Production and Emissions, Energy Storage, Plasma Cutting and Welding, Non-Newtonian Fluids and Drag Reduction and their Biomedical Applications and Polymers Processing and Manufacturing.